Eur. Phys. J. A (2021) 57:87
https://doi.org/10.1140/epja/s10050-021-00405-y

THE EUROPEAN PHYSICAL JOURNAL A

Regular Article - Theoretical Physics

Towards a systematic optical model potential for A = 8 projectiles

Y. Kucuk[1,a], **V. Guimarães**[2,b], **B. V. Carlson**[3,c]

[1] Department of Physics, Akdeniz University, Antalya, Turkey
[2] Instituto de Física, Universidade de São Paulo, Rua do Matão 1371, São Paulo, SP 05508-090, Brazil
[3] Instituto Tecnológico de Aeronáutica, 12.228-900 São José dos Campos, São Paulo, Brazil

Received: 23 December 2020 / Accepted: 19 February 2021 / Published online: 5 March 2021

Communicated by Nicolas Alamanos

Abstract An optical model analysis of the available data for A = 8 (^{8}He, ^{8}Li and ^{8}B) projectiles on different targets with light, medium and heavy mass has been performed. A systematic potential set based on a Woods–Saxon Potential shape was obtained. This potential describes the elastic scattering angular distributions quite well. A more physical model within the framework of a semi-microscopic approach, where the nuclear matter density distributions of the ^{8}B, ^{8}Li and ^{8}He projectiles have been calculated by using a microscopic self-consistent relativistic mean field (RMF) theory, was also considered. The agreement of the calculated angular distributions with the data was reasonable. An improvement of the agreement could be achieved by changing the imaginary diffuseness parameter, which is a sensitive parameter in these calculations.

1 Introduction

With the advent of facilities to produce light radioactive beams, investigation of the interactions and structure of exotic nuclei have been studied extensively [1]. These investigations have revealed that some weakly-bound unstable nuclei, called exotic nuclei, exhibit characteristic features, such as a halo or Borromean structures, as well as a soft dipole excitation mode. An extensive review of the investigation of halo nuclei can be found in Ref. [2], where a discussion of experimental methods used to determine the exotic nature of some of these nuclei is presented. The concept defining a halo nucleus is the combination of a long tail in the density distribution and a certain degree of decoupling between the core and valence nucleons. Halos have been observed either in the form of one-nucleon halos, as in ^{8}B and ^{11}B, or two-nucleon halos, as in ^{6}He and ^{11}Li, which, in the latter cases, may form a Borromean structure. For a Borromean halo, the spatial correlation between two-halo neutrons is an important issue. In this sense, the radius and the matter distribution play important roles in the structure of these nuclei. Apart from specific structure effects, the shape of the nuclear density for stable nuclides is nearly a Fermi distribution, with the diffuseness approximately constant and a radius given roughly by $R = r_0 \times A^{1/3}$, where A is the number of nucleons in the nucleus and $r_0 \approx 1.3$ fm. However, the situation changes for light weakly-bound and exotic nuclei where clustering phenomena are quite important.

In this work, we consider the A = 8 projectiles (^{8}He, ^{8}Li and ^{8}B), which are a quite interesting special case. They are all radioactive, since there is no stable nucleus with mass A = 8, and weakly-bound. The ^{8}He projectile, with a $2n$ separation energy of $S_{2n} = 2.140$ MeV and $J = 0^+$, is the the most neutron-rich particle-stable nucleus known, with $N/Z = 3$. Several experiments based on its interaction cross section and proton scattering in inverse kinematics have been performed to investigate the structure of ^{8}He. An extensive review of these experiments has been performed by Lapoux and Alamanos in Ref. [3]. The conclusion of this review, combined with the conclusion from the interaction cross section measurements of Ref. [4], is that ^{8}He is more like a 4n skin nucleus with a ^{4}He core rather than a ^{6}He+2n configuration. However, as the remaining ^{7}He nucleus is unbound when one neutron is removed, it can also be considered to have a Borromean structure. Elastic scattering for ^{8}He on ^{208}Pb has been measured at an energy close to the Coulomb barrier [5]. An analysis in terms of a coupled reaction channel (CRC) model with a Dipole Polarization Potential indicates that the absorption due to single-neutron stripping takes place at large radii [6]. On the other side of the isotopic chain, one has the ^{8}B nucleus. It is a proton-rich nucleus with $J^\pi = 2^+$ and with

[a] e-mail: ykucuk@akdeniz.edu.tr
[b] e-mail: valdir.guimaraes@usp.br;valdirg@if.usp.br (corresponding author)
[c] e-mail: brett@ita.br

the lowest proton binding energy known for a bound nucleus, with $S_p = 0.138$ MeV, for the ^{7}Be+p decay. This nucleus has been found to have a proton halo configuration and the recent intermediate energy proton elastic scattering measurement, in inverse kinematics, performed for ^{8}B, is the most striking evidence in favor of the proton halo configuration [7]. The ^{8}Li nucleus is the mirror of ^{8}B, also with $J^\pi = 2^+$ and with a neutron binding energy of $S_n = 2.032$ MeV, for the ^{7}Li+n decay. In terms of its configuration, the ^{8}Li nucleus closely resembles the other lithium isotopes [8]. Its binding energy is not so small ($S_n = 2.032$ MeV), it is not a very neutron-rich nucleus ($N/Z = 1.7$), and it has no anomalous structure.

In terms of experiments, an effort has been made by several laboratories to improve the intensity of their radioactive ion beams. We can thus expect high precision measurements of reaction channels induced by radioactive beams such as ^{8}B, ^{8}Li and ^{8}He in the near future. These measurement will be very welcome and they will permit the investigation of finer details, such as deformation and core excitation in the transfer, breakup and fusion channels. To help in this further analysis, it will be important to establish a good global optical potential for the radioactive nuclei. In the present work we report on a phenomenological analysis of available elastic scattering data with A = 8 projectile. To this end we investigated the possibility of establishing a global potential set to describe elastic scattering for the ^{8}B, ^{8}Li and ^{8}He projectiles from light to heavy target nuclei at low energies.

Although a well understood process, elastic scattering still attracts considerable interest due to its role in the investigation of the exotic features of halo nuclei, such as ^{6}He, ^{8}B, ^{11}Li and ^{11}Be [1,9]. At low energy, cross sections for the elastic process are quite large and the process is quite appropriate to be used in association with radioactive ion beams, where the beam intensities are limited. The unusual features of exotic nuclei, such as a strong cluster configuration, small binding energy and a large interaction cross section, are expected to manifest themselves in the elastic scattering angular distributions. For neutron-rich nuclei such as ^{11}Be and ^{11}Li, the coupling effect is quite strong due to the Coulomb dipole polarizability for ^{11}Li [10,11] and the nuclear potential for ^{11}Be [12,13]. The coupling effect due to the Coulomb dipole is observed in the angular distribution of the elastic scattering in the damping of the Fresnel peak (nuclear-Coulomb interference peak). For proton-rich ^{8}B, on other hand, the dipole polarizability is suppressed (due to confinement of the valence proton inside its Coulomb and centrifugal barrier) and the effect of the absorption in the angular distribution is expected to be smaller [14,15] Analysis of elastic scattering angular distributions measured at energies near the Coulomb barrier can thus provide valuable information on both the static and dynamical effects of weakly-bound nuclei.

The phenomenological approach, in which the interaction between the colliding nuclei is represented by a complex optical-model potential, is a very reliable and practical method to analyze elastic scattering data. In this approach, the intrinsic properties of the collision partners are not explicitly taken into account. On the other hand, the description of the cross sections for elastic scattering is very sensitive to the interaction potential between the projectile and the target nuclei and, thus, to the structure of the nuclei involved in the collision. In the end, the strong synergy between the configuration of the projectile and dynamics of the process involved in reactions induced by exotic and weakly bound (stable and radioactive) nuclei makes elastic scattering a powerful tool for investigating the effect of cluster configurations of weakly-bound and exotic nuclei. For nuclei with a halo structure and low binding energy, the breakup and transfer reactions may strongly compete with the elastic scattering process. Due to the low binding energy, the cluster configurations in these weakly bound nuclei can produce strong couplings to the continuum, introducing a characteristic dynamic polarization (attractive or repulsive) in the optical potential.

Global and systematic potentials have been developed and are quite helpful in the analysis of elastic and reaction data. Several old and new generations of such potentials have been extensively used over the past years [16–23] in elastic and reaction data analyses. Most of these global optical potentials were developed for light particles and assume that the depths, radii and diffuseness parameters of the optical potentials have a simple dependence on the incident energy and mass of the target. Few of these potentials embrace a wide range of projectiles. The reason is exactly the difference in the cluster configurations of the several projectiles, which can introduce different effects in the elastic scattering due to the reaction dynamics, such as strong collective excitation, breakup, and transfer reactions. Also, in the elastic scattering analysis with an optical model, the partial waves are mostly sensitive to the tail region of the potential, and, thus, we can expect that several sets of parameters that maintain a similar potential shape in the tail region would give equivalent fits to the data [24]. However, by considering a wide range of masses for the projectile and/or target, global or systematic potentials may reduce these ambiguities in the optical model potential. In this present work we perform optical model calculations with the aim of obtaining a general and systematic potential set for A = 8 projectile.

The organization of this paper is as follows. In Sect. 2, the method and formalism used in the present work are described in detail. A new set of A = 8 OMP parameters is presented and comparison with the experimental data is exhibited. In Sect. 3, the results of the double-folding analysis with calculated densities are presented. Finally, we present a summary of the results and the conclusions of the study in Sect. 4.

Table 1 Systems considered in the present work and their corresponding references. The cross sections were extracted from the EXFOR database [26]. Those indicated by asterisks were obtained directly from the author of the corresponding work

System	E_{Lab} (MeV)	References
^{8}B+^{12}C	25.8	Barioni-11 [27]
^{8}B+^{27}Al (*)	15.3, 21.7	Morcelle-17 [28]
^{8}B+^{58}Ni	20.7, 23.4, 25.3, 27.2, 29.3	Aguilera-09 [29]
^{8}B+^{208}Pb (*)	50.0	Mazzocco-19 [30]
^{8}B+^{208}Pb	178.0	Yang-18 [31]
^{8}He+^{208}Pb	16.0, 22.0	Duran-18 [5]
^{8}Li+^{12}C	14.0	Becchetti-93 [32]
^{8}Li+^{12}C	23.9	Barioni-09 [33]
^{8}Li+^{58}Ni	19.6	Becchetti-93 [32]
^{8}Li+^{58}Ni (*)	26.1	Santos-19 [34]
^{8}Li+^{90}Zr	18.5, 21.5	Pakou-15 [35]
^{8}Li+^{208}Pb	25.3, 29.0, 30.0, 34.4	Kolata-02 [36]
^{8}Li+^{209}Bi	38.2, 39.9, 40.9	Cook-18 [37]

2 Optical model analysis

In this paper we perform optical model calculations with the aim of obtaining a systematic potential set for A = 8 projectiles. For this purpose, we analyze several experimental elastic scattering angular distributions (ratio to Rutherford) for ^{8}B, ^{8}Li and ^{8}He on different targets, as listed in Table 1.

The total effective potential in the optical model consists of the Coulomb, centrifugal, and nuclear potentials:

$$V_{total}(r) = V_{Nuclear}(r) + V_{Coulomb}(r) + V_{Centr}(r), \quad (1)$$

where, the Coulomb and centrifugal potentials are well known. The Coulomb potential [38] due to a charge $Z_P e$ interacting with a charge $Z_T e$ distributed uniformly over a sphere of radius R_c is given by:

$$\begin{aligned} V_{Coulomb}(r) &= \frac{1}{4\pi\epsilon_0}\frac{Z_P Z_T e^2}{r}, r \geq R_C \\ &= \frac{1}{4\pi\epsilon_0}\frac{Z_P Z_T e^2}{r}\left(3 - \frac{r^2}{R_C^2}\right), r < R_C \end{aligned} \quad (2)$$

where R_C is the Coulomb radius, taken as $r_{0C} \times (A_P^{1/3} + A_T^{1/3})$ fm, with $r_{0C} = 1.24$, in our calculations, and Z_P and Z_T the charges of the projectile (target) P(T) nuclei, respectively.

The centrifugal potential is given by:

$$V_{Centr}(r) = \frac{\hbar^2 l(l+1)}{2\mu r^2} \quad (3)$$

where μ is the reduced mass of the colliding pair.

2.1 OM with Woods–Saxon potentials

For the real and imaginary parts of the complex $V_{nuclear}(r)$ potential, we first considered a Woods–Saxon form as shown in Eq. 4 below.

$$\begin{aligned} V_N(R) = &\frac{V_0}{1 + \exp(R - R_V)/a_V]} \\ &+ i\,\frac{W_0}{1 + \exp[(R - R_W)/a_W]}, \end{aligned} \quad (4)$$

where $R_{V,W} = r_{V,W}\,(A_P^{1/3} + A_T^{1/3})$, A_P and A_T are the mass numbers of the projectile and target nuclei.

This complex Woods–Saxon potential has six parameters to be adjusted. After checking the parameters used in the original publication of each data set listed in Table 1, we decided to consider the depth for the real and imaginary potentials, $V_0 = 250$ MeV and $W_0 = 10$ MeV, respectively, as well as the diffuseness parameters, $a_V = a_W = 1.0$ fm as fixed parameters and to search for the best radius parameters. The best values obtained for the reduced radii were $r_v = 0.75$ fm and $r_W = 1.25$ fm. A fine tuning of the diffuseness parameters was then performed by searching for the values that would give the minimum chi-square for each energy data set. The final values obtained for all the systems are listed in Table 2. It is important to mention that our analysis shows a stronger sensitivity to the diffuseness parameter (real and imaginary) than to the radius parameters, which was the reason these parameters were chosen for the fine tuning.

The result of this Woods–Saxon optical potential analysis is shown by the solid black lines in Fig. 1 for the ^{8}B+^{12}C and ^{8}B+^{27}Al systems, in Fig. 2 for the ^{8}B+^{58}Ni system, in Fig. 3 for the ^{8}B+^{208}Pb and ^{8}He+^{208}Pb systems, in Fig. 4 for the ^{8}Li+^{12}C system, in Fig. 5 for the ^{8}Li+^{58}Ni and ^{8}Li+^{90}Ar systems and in Fig. 6 for the ^{8}Li+^{208}Pb and ^{8}Li+^{209}Bi systems. As observed in the figures, this systematic potential describes all of the data sets quite well. Also, as seen from the table, the diffuseness parameter of the real part varies from 0.5 to 1.0 fm, while the diffuseness parameter of the imaginary part varies from 0.75 to 1.40 fm. The larger values for the imaginary diffuseness parameter, obtained for all A = 8 projectiles on the ^{208}Pb target, might be an indication of the importance of the absorption due to the coupling to direct reactions such as breakup and/or transfer. It is also important to mention that due to the lack of data spanning a broader range of energy, it was not possible to establish an energy dependence for the parameters, as for instance, that obtained for the ^{9}Be projectile in Ref. [23].

The need to change the diffuseness parameter to improve the agreement between the calculation and the data might also be an indication that the density distributions for these

Table 2 Systems considered in the present analysis extracted from EXFOR [26]. The Woods–Saxon potential parameters are: V = 250 MeV, W = 10 MeV, r_V = 0.75 fm, r_W = 1.25 fm

System	Energies E_{Lab} (MeV)	a_V	a_W
^{8}B+^{12}C	25.8	0.75	1.00
^{8}B+^{27}Al	15.3	0.75	1.00
	21.7	0.95	0.90
^{8}B+^{58}Ni	20.7	0.60	1.05
	23.4	0.60	1.05
	25.3	0.55	1.01
	27.2	0.60	1.10
	29.2	0.60	1.00
^{8}B+^{208}Pb	50.0	0.80	1.25
	178.0	1.00	1.25
^{8}He+^{208}Pb	16.0	0.80	1.35
	22.0	0.80	1.40
^{8}Li+^{12}C	14.0	0.60	1.00
	23.9	0.50	1.00
^{8}Li+^{58}Ni	19.6	0.9	0.9
	26.1	0.65	0.75
^{8}Li+^{90}Zr	18.5	1.05	0.80
	21.5	1.00	0.80
^{8}Li+^{208}Pb	25.3	1.1	1.30
	29.0	1.0	1.20
	30.0	0.75	1.25
	34.4	0.75	1.30
^{8}Li+^{209}Bi	38.2	1.0	0.95
	39.9	1.0	0.95
	40.9	1.0	0.90

projectiles might play an important role in the elastic scattering.

2.2 OM with phenomenological potential

To perform an optical model analysis on the available data with a more physical model, we have also considered the framework of the semi-microscopic approach. In this model the real part of the complex optical potential is given by a double folding potential, while the imaginary part is a Woods–Saxon shaped potential with the parameters W_0 = 10 MeV, a_W = 1.0 fm and r_W = 1.25 fm. This imaginary potential is the same as the one used in the previous analysis. The complex nuclear potential in this model is then given by:

$$V_N(R) = N_R\, V_{DF}(R) + i\, \frac{W_0}{1 + \exp\left[(R - R_W)/a_W\right]}, \qquad (5)$$

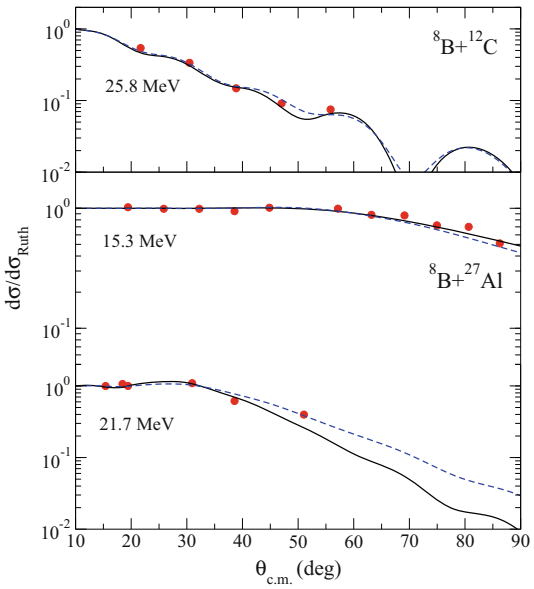

Fig. 1 Elastic scattering angular distributions for the ^{8}B+^{12}C [27] and ^{8}B+^{27}Al [28] systems. The black solid line is the result with the Woods–Saxon potential and the blue dashed line is the result of the phenomenological potential described in the text

where $V_{DF}(R)$ is the double folding potential, which is evaluated by folding the nuclear matter distributions with the effective nucleon-nucleon interaction (v_{nn}):

$$V_{DF}(R) = \int d\mathbf{r}_1 \int d\mathbf{r}_2\, \rho_p(\mathbf{r}_1)\, \rho_t(\mathbf{r}_2)\, v_{NN}(\mathbf{r}_{12}), \qquad (6)$$

where $\rho_P(\mathbf{r}_1)$ and $\rho_T(\mathbf{r}_2)$ are the nuclear matter densities of the projectile and target nuclei, $\mathbf{r}_{12} = \mathbf{R} - \mathbf{r}_1 + \mathbf{r}_2$ and N_R is the normalization factor.

The nuclear matter density distributions for the ^{8}B, ^{8}Li and ^{8}He projectiles have been calculated by using a microscopic self-consistent relativistic mean field (RMF) model with the DD-ME2 interaction [39,40]. The density distribution for each of these projectiles is shown in Fig. 7. As can be observed in the figure, the density for the neutron-rich isobar, ^{8}He, is the one with the largest spacial extension. This is actually compatible with the large values of the imaginary diffuseness parameter obtained for ^{8}He in the previous Woods–Saxon potential analysis. The density distributions for the targets, ^{27}Al, ^{58}Ni, ^{90}Zr, ^{208}Pb and ^{200}Bi, were taken from Hartree–Fock–Bogolubov (HFB) calculations based on the BSk2 Skyrme force [41].

The matter density distribution for ^{12}C has been assumed to be a two-parameter Fermi function:

$$\rho_T(r_1) = \frac{\rho_0}{1 + exp(\frac{r_1 - a}{c})}, \qquad (7)$$

where the parameters ρ_0, a and c have been chosen to reproduce the rms matter radius of ^{12}C [42].

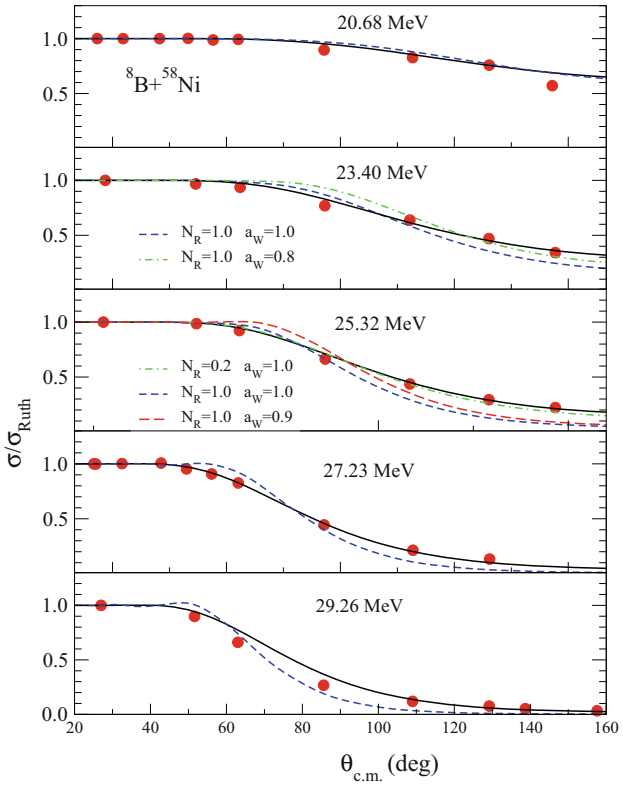

Fig. 2 Elastic scattering angular distributions for the ^{8}B+^{58}Ni system [29]

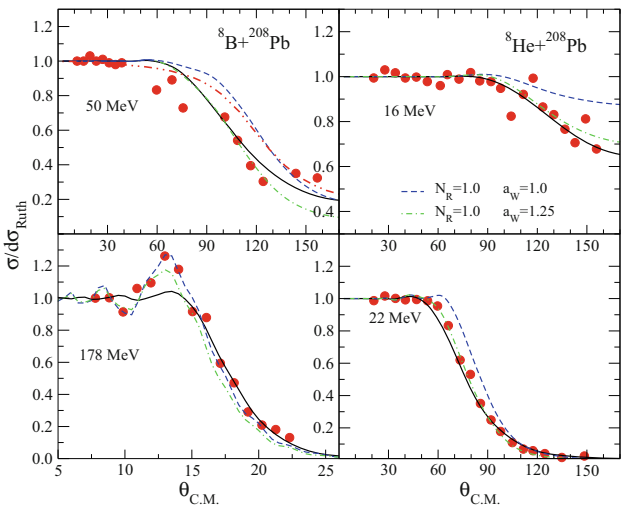

Fig. 3 Elastic scattering angular distributions for the ^{8}B+^{208}Pb [30,31] and ^{8}He+^{208}Pb [5] systems. The double-dot dashed line corresponds to the CDCC calculation for the ^{8}B+^{208}Pb system extracted from Ref. [30]

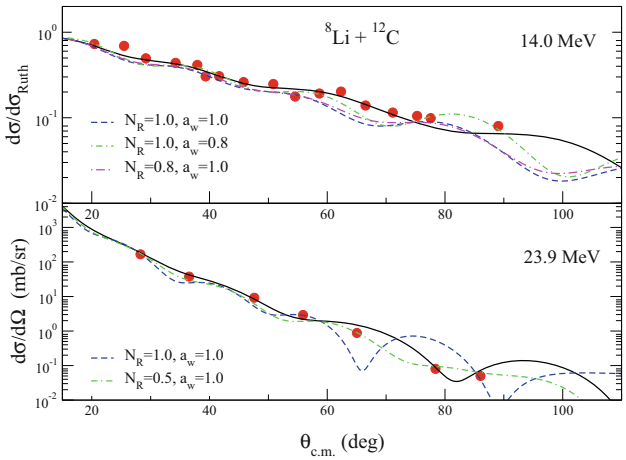

Fig. 4 Elastic scattering angular distributions for the ^{8}Li+^{12}C system at 14.0 MeV [32] and at 23.9 MeV [33]

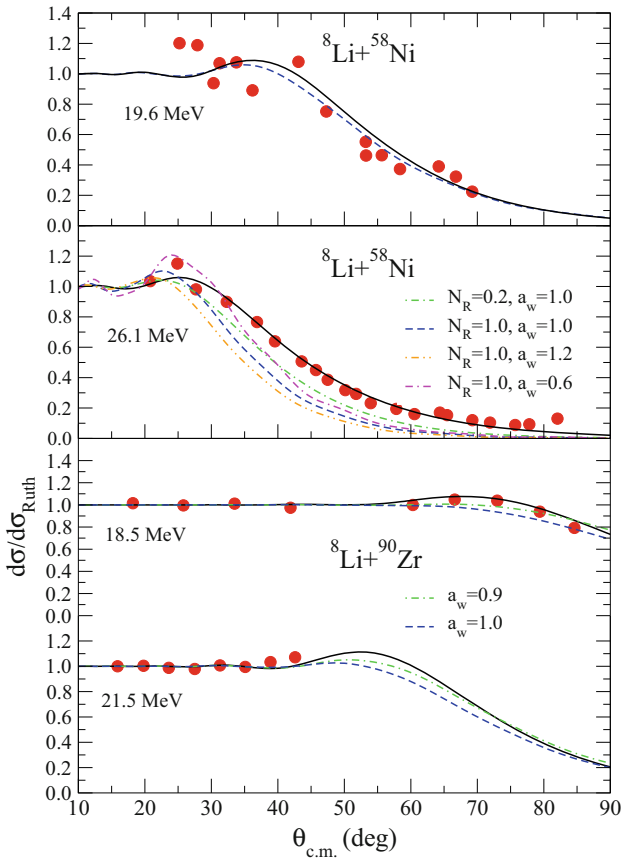

Fig. 5 Elastic scattering angular distributions for the ^{8}Li+^{58}Ni at 19.6 MeV [32] and at 26.1 MeV [34], and for ^{8}Li+^{90}Zr [35] systems

We have chosen the realistic Michigan-three-range-Yukawa ($M3Y$) effective nucleon–nucleon interaction [43]:

$$v_{NN}(r) = 7999\frac{e^{-4r}}{4r} - 2134\frac{e^{-2.5r}}{2.5r} + J_{00}(E)\,\delta(\mathbf{r}), \qquad (8)$$

where $J_{00}(E)$ represents the exchange term, since nucleon exchange is possible between projectile and target. $J_{00}(E)$ has a linear energy-dependence and is expressed as

$$J_{00}(E) = 276\,[1 - 0.005\,E/A_P]\,(\text{MeV}). \qquad (9)$$

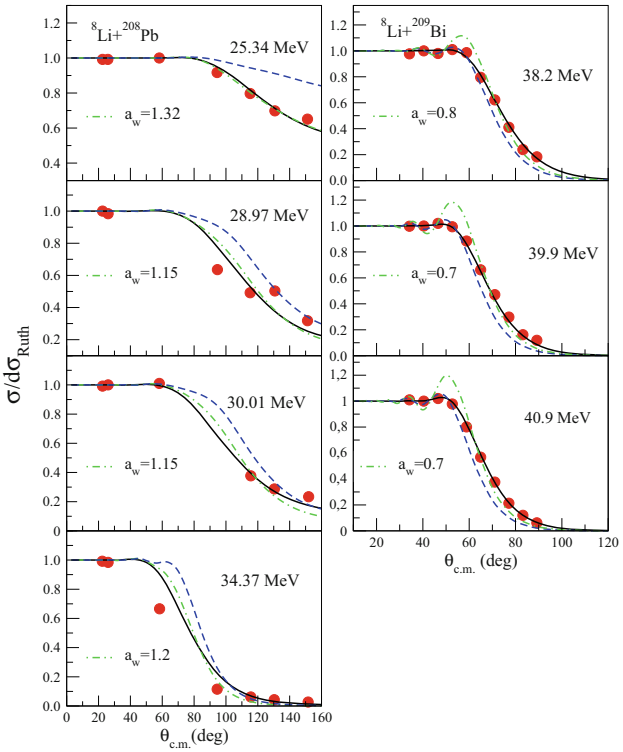

Fig. 6 Elastic scattering angular distributions for the ^{8}Li+^{208}Pb [36] and ^{8}Li+^{209}Bi [37] systems

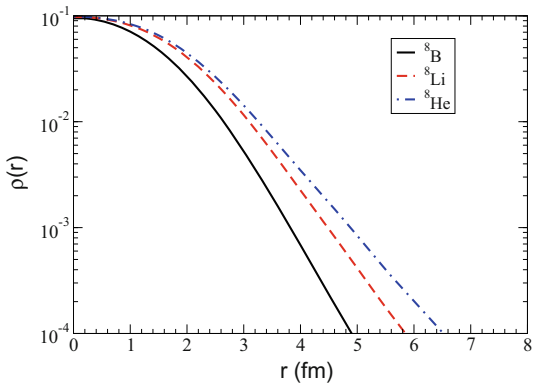

Fig. 7 Density for the ^{8}B, ^{8}Li and ^{8}He projectiles

Using the above phenomenological potential model we have calculated the elastic-scattering angular distributions for the ^{8}B, ^{8}Li and ^{8}He projectiles on several targets with low, medium and heavy mass. The calculations with the present potential model are compared to the experimental angular distributions in Figs. 1, 2, 3, 4 5 and 6. The blue dashed lines in the figures correspond to the calculation without any change in the parameters. In general, the agreement between the calculated cross sections and the elastic data can be considered reasonably good. This can also be considered an important achievement since the projectiles have completely different configurations. Next we discuss with more details the results for each projectile.

For ^{8}B on the light targets, ^{12}C and ^{27}Al, the agreement of the calculation, using the phenomenological potential, the blue dashed line, with the elastic data is very good, see Fig. 1. Actually, the agreement is better with the phenomenological potential than with the systematic adjusted Woods-Saxon potential (solid black line). For the ^{8}B+^{58}Ni system the agreement with the phenomenological potential and the data is poorer, as can be seen by the blue dashed line in Fig. 2. Since the imaginary diffuseness parameter in the previous analysis with Woods–Saxon potential was shown to be quite sensitive in the calculation, we decided to change this parameter slightly. The agreement of the calculation with the angular distribution at incident energy E_{Lab} = 23.40 MeV improved by changing a_W from 1.0 to 0.8 fm. However, for the incident energy E_{Lab} = 25.32 MeV, good agreement was achieved only by changing the normalization of the real part (given by a double-folding potential) from N_R = 1.0 to N_R = 0.2, as shown by the green dot-dashed line in Fig. 2. The need of a shallower potential to describe the data might be an indication that a repulsive real surface polarization potential, related to the effect of breakup on the elastic scattering, might be important to describe the data.

For the ^{8}B+^{208}Pb system, shown in Fig. 3, the phenomenological potential describes the data quite well at higher incident energy (3 times the Coulomb Barrier), including the Fresnel peak region. However, our phenomenological potential, given by the dashed blue line, could not describe the data at energy close to the Coulomb barrier, where strong absorption is evident. Improvement of the agreement can be achieved simply by changing the imaginary diffuseness parameter from a_W = 1.0 fm to 1.25 fm. The strong absorption for this system has already been discussed in Ref. [30]. Although, breakup has been found to be quite strong at sub-barrier energies, as reported in Ref. [44], the continuum discretization coupled channel (CDCC) calculations, which would take into account the influence of the elastic breakup in the angular distribution, failed to reproduce these data. This has been considered by the authors as due to the limitation in the description of ^{8}B as an inert core of ^{7}Be plus a valence proton particle. More data for ^{8}B elastic scattering and breakup on heavy targets at energies close to the Coulomb barrier would be very welcome to better understand the reason for the strong absorption.

For ^{8}He projectile there is only one set of data measured with the ^{208}Pb target, at two incident energies close to the Coulomb barrier (slightly above and slightly below). Our phenomenological potential surprisingly describes the data measured above the Coulomb barrier better than that below, where we would expected less influence of the nuclear potential. It would be interesting to see if the phenomenological potential can describe data obtained at higher energies.

Again, improvement of the agreement with the low energy data has been achieved by changing the imaginary diffuseness parameter from a_W = 1.0 fm to 1.25 fm, as shown by the green dot-dashed line in Fig. 3.

The results for ^{8}Li in the light ^{12}C target are shown in Fig. 4. Our phenomenological potential gives a reasonable description of the data. Small improvement could be obtained by changing the imaginary diffuseness parameter for the lower energy data set and the normalization of the real part for the higher energy data set, as indicated in the figure. Data for ^{8}Li on medium (^{58}Ni and ^{90}Zr) targets is present in Fig. 5. As can be seen in the figures, our phenomenological potential could describe well the data for the ^{8}Li+^{58}Ni system at 19.6 MeV, where the data is more scattered, but it could not describe the elastic data for the higher energy, 26.1 MeV. For the ^{90}Zr target, an improvement has been achieved by changing the imaginary diffuseness parameter, as indicated in the figure. However, for the ^{8}Li+^{58}Ni system at 26.1 MeV the situation is quite complicated. Usually, folding potentials tend to overestimate the experimental data at backward angles. For this data set, the folding model underpredicts the cross section at backward angles. We have tried to change the imaginary diffuseness parameter as well as the normalization of the real part of the optical potential. It seems that to improve the agreement a shallower real potential is required. The authors in Ref. [34] have considered the spin-orbit effect to explain the data, since $J^{\pi} = 2^{+}$ for ^{8}Li. Coupled-channel analyses for the elastic scattering of ^{8}Li have shown that neutron transfer reactions are quite important to describe the elastic scattering data [35,36]. Our optical potential model could not reproduce this effect, indicating the necessity of extra surface terms in the potential.

For the ^{208}Pb target, our model overpredicts the cross sections at backward angles. Thus, increasing the diffuseness parameter was enough to increase the absorption and improve the description of the data, as can be seen in Fig. 6. However, for the ^{58}Ni and ^{209}Bi targets, our model underpredicted the cross sections at backward angles. Using a smaller value for the diffuseness parameter decreases the absorption at backward angles, improving the agreement with the data in this angular region, but also produces less absorption at the Fresnel peak, as can be seen for the ^{209}Bi target in Fig. 6. The observed damping of the Fresnel peak in the data for the ^{8}Li+^{209}Bi is an indication of strong absorption at more forward angles, possible due to a neutron transfer reaction as observed in Ref. [35]. Using our phenomenological model calculation as a benchmark, we can see that there is a target effect in the elastic data for ^{8}Li+^{208}Pb and ^{8}Li+209Bi systems. This might be an indication that coupling effects due to transfer reactions might be stronger for the ^{209}Bi target.

3 Summary

We present a set of potentials for A = 8 (^{8}He, ^{8}Li and ^{8}B) projectiles based on the traditional Woods–Saxon potential shape and on a phenomenological potential, which consists of a mixing of a double-folding potential for the real part and a Woods–Saxon form for the imaginary part of the complex potential. The parameters of the Woods–Saxon based potential were obtained by performing a systematic analysis on the data available for the ^{8}B, ^{8}Li and ^{8}He projectiles on several targets of light, medium and heavy mass. This systematic potential was found to be sensitive to the real and imaginary diffuseness parameters. This systematic potential might be useful in further calculations of reactions using these projectiles. We also developed a phenomenological potential considering a real double-folding potential and imaginary Woods–Saxon imaginary potential. The double-folding potential consisted of the $M3Y$ nucleon–nucleon interaction folded with densities calculated using a microscopic self-consistent relativistic mean field (RMF) theory. Comparisons with the experimental data show that the calculated angular distributions are in good agreement with the existing experimental data. For some angular distributions, a fine tuning on the imaginary diffuseness parameter was necessary to better describe the data. However, for ^{8}B+^{58}Ni and ^{8}Li+^{58}Ni systems an extra modification to a shallower real potential was also necessary to better describe the data. This might be an indication of the importance of a repulsive real surface polarization potential, possibly due to effect of direct reactions (transfer and/or breakup) in the elastic scattering of these systems. We should emphasize that these projectiles are all radioactive and ^{8}B and ^{8}He are considered exotic nuclei. The obtained phenomenological potential should thus also be considered in further analyses of reactions induced by these projectiles. The procedure applied here can be applied to other halo-type nuclei and a similar analysis for the ^{10}C, ^{10}B and ^{10}Be projectiles is under development. The contribution of Professor Hussein to scattering theory is quite extensive [9,45–51]. With this work we intend to honor his memory and legacy in the field.

Acknowledgements The authors would like to thank São Paulo Research Foundation (FAPESP) (Grants 2016/17612-7 and 2017/05660-0) and the Conselho Nacional de Desenvolvimento Científico (CNPq) (Grants 304961/2017-5 and 306433/2017-6) for the financial support. The authors also thank INCT-FNA (Instituto Nacional de Ciência e Tecnologia- Física Nuclear e Aplicações, research project 464898/2014-5).

Data Availability Statement This manuscript has no associated data or the data will not be deposited. [Authors' comment: No new experimental data were presented in this paper. The data were obtained from the EXFOR data library or directly from the authors who published them as in Table 1.]

References

1. J.J. Kolata, V. Guimarães, E.F. Aguilera, Elastic scattering, fusion, and breakup of light exotic nuclei. Eur. Phys. J. A **53**, 123 (2016)
2. I. Tanihata, H. Savajols, R. Kanungo, Recent experimental progress in nuclear halo structure studies. Prog. Part. Nucl. Phys. **68**, 215 (2013)
3. V. Lapoux, N. Alamanos, Weakly bound Borromean structures of the exotic ^{6,8}He nuclei through direct reactions on proton. Eur. Phys. J. A **51**, 91 (2015)
4. I. Tanihata, D. Hirata, T. Kobayashi, S. Shirnoura, K. Sugimoto, H. Toki, Revelation of thick neutron skins in nuclei. Phys. Lett. B **289**, 261 (1992)
5. G. Marquinez-Duran, I. Martel, A.M. Sanchez-Benitez, L. Acosta, J.L. Aguado, R. Berjillos, A.R. Pinto, T. Garcia, J.A. Duenas, K. Rusek, N. Keeley, K.W. Kemper, M.A.G. Alvarez, M.J.G. Borge, A. Chbihi, C. Cruz, M. Cubero, J.P. Fernandez-Garcia, B. Fernandez-Martinez, J.L. Flores, J. Gomez-Camacho, J.A. Labrador, F.M. Marques, A.M. Moro, M. Mazzocco, A. Pakou, V.V. Parkar, N. Patronis, V. Pesudo, D. Pierroutsakou, R. Raabe, R. Silvestri, N. Soic, L. Standylo, I. Strojek, O. Tengblad, R. Wolski, Z. Abou-Haidar, Interaction of ^{8}He with ^{208}Pb at near-barrier energies: ^{4}He and ^{6}He production. Phys. Rev. C **98**, 034615 (2018)
6. G. Marquinez-Duran, N. Keeley, K.W. Kemper, R.S. Mackintosh, I. Martel, K. Rusek, A.M. Sanchez-Benitez, Influence of single-neutron stripping on near-barrier ^{6}He+^{208}Pb and ^{8}He+^{208}Pb elastic scattering. Phys. Rev. C **95**, 024602 (2016)
7. G.A. Korolev, A.V. Dobrovolsky, A.G. Inglessi, G.D. Alkhazov, P. Egelhof, A. Estrade, I. Dillmann, F. Farinon, H. Geissel, S. Ilieva, Y. Ke, A.V. Khanzadeev, O.A. Kiselev, J. Kurcewicz, X.C. Le, YuA Litvinov, G.E. Petrov, A. Prochazka, C. Scheidenberger, L.O. Sergeev, H. Simon, M. Takechib, S. Tang, V. Volkov, A.A. Vorobyov, H. Weick, V.I. Yatsoura, Halo structure of ^{8}B determined from intermediate energy proton elastic scattering in inverse kinematics. Phys. Lett. B **780**, 200 (2018)
8. G. W. Fan, M. Fukuda, D. Nishimura, X. L. Cai, S. Fukuda, I. Hachiuma, C. Ichikawa, T. Izumikawa, M. Kanazawa, A. Kitagawa, T. Kuboki, M. Lantz, M. Mihara, M. Nagashima, K. Namihira, Y. Ohkuma, T. Ohtsubo, Zhongzhou Ren, S. Sato, Z. Q. Shen, M. Sugiyama, S. Suzuki, T. Suzuki, M. Takechi, T. Yamaguchi, B. J. Xu, and W. Xu. Structure of8Li from a reaction cross-section measurement. Phys. Rev. C **90**, 044321 (2014)
9. L.F. Canto, V. Guimaraes, J. Lubian, M.S. Hussein, The total reaction cross section of heavy-ion reactions induced by stable and unstable exotic beams: the low-energy regime. Eur. J. Phys. A **56**, 281 (2020)
10. M. Cubero, J.P. Fernández-García, M. Rodríguez-Gallardo, L. Acosta, M. Acorta, M.A.G. Alvarez, M.J.G. Borge, L. Buchmann, C.A. Diget, H.A. Falou et al., Do halo nuclei follow rutherford elastic scattering at energies below the barrier? The case of ^{11}Li. Phys. Rev. Lett. **109**, 262701 (2012)
11. N. Keeley, K.W. Kemper, K. Rusek, Dynamic polarization potentials and dipole polarizabilities of ^{11}Li, ^{6}He and ^{6}Li compared. Phys. Rev. C **88**, 017602 (2013)
12. A. Di Pietro, V. Scuderi, A.M. Moro, L. Acosta, F. Amorini, M.J.G. Borge, P. Figuera, M. Fisichella, L.M. Fraile, J. Gomez-Camacho, H. Jeppesen, M. Lattuada, I. Martel, M. Milin, A. Musumarra, M. Papa, M.G. Pellegriti, F. Perez-Bernal, R. Raabe, G. Randisi, F. Rizzo, G. Scalia, O. Tengblad, D. Torresi, A.M. Vidal, D. Voulot, F. Wenander, M. Zadro, Experimental study of the collision ^{11}Be + ^{64}Zn around the Coulomb barrier. Phys. Rev. C **85**, 054607 (2012)
13. A. Di Pietro, G. Randisi, V. Scuderi, L. Acosta, F. Amorini, M. J. G, Borge, P. Figuera, M. Fisichella, L. M. Fraile, J. Gomez-Camacho, H. Jeppesen, M. Lattuada, I. Martel, M. Milin, A. Musumarra, M. Papa, M. G. Pellegriti, F. Perez-Bernal, R. Raabe, F. Rizzo, D. Santonocito, G. Scalia, O. Tengblad, D. Torresi, A. M. Vidal, D. Voulot, F. Wenander, M. Zadro. Elastic scattering and reaction mechanisms of the halo nucleus ^{11}Be around the Coulomb Barrier. Phys. Rev. Lett. **105**, 022701 (2010)
14. Y.Y. Yang, X. Liu, D.Y. Pang, Distinction between elastic scattering of weakly bound proton- and neutron-rich nuclei: the case of ^{8}B and ^{11}Be. Phys. Rev. C **94**, 034614 (2016)
15. J. Rangel, J. Lubian, L.F. Canto, P.R.S. Gomes, Effect of Coulomb breakup on the elastic cross section of the ^{8}B proton-halo projectile on a heavy, ^{208}Pb target. Phys. Rev. C **93**, 054610 (2016)
16. F.D. Becchetti Jr., G.W. Greenlees, Nucleon–nucleus optical-model parameters, A>40, E<50 MeV. Phys. Rev **182**, 1190 (1969)
17. B.A. Watson, P.P. Singh, R.E. Segel, Optical-model analysis of nucleon scattering from 1p-shell nuclei between 10 and 50 MeV. Phys. Rev. **182**, 977 (1969)
18. J. Cook, Global optical-model potentials for the elastic scattering of ^{6,7}Li projectiles. Nucl. Phys. A **388**, 153 (1982)
19. R.L. Varner, W.J. Thompson, T.L. McAbee, E.J. Ludwig, T.B. Clegg, A global nucleon optical model potential. Phys. Rep. **201**, 57 (1991)
20. A.J. Koning, J.P. Delaroche, Local and global nucleon optical models from 1 keV to 200 MeV. Nucl. Phys. A **713**, 231 (2003)
21. D. Y. Pang, P. Roussel-Chomaz, H. Savajols, R. L. Varner, R. Wolski. Global optical model potential for A = 3 projectiles. Phys. Rev. C **79**, 024615 (2009), Erratum Phys. Rev. C **81**, 019902 (2010)
22. Y.P. Xu, D.Y. Pang, Toward a systematic nucleus-nucleus potential for peripheral collisions. Phys. Rev. C **87**, 044605 (2013)
23. X. Yongli, Y. Han, H. Liang, W. Zhendong, H. Guo, Chonghai Cai, Global optical model potential for the weakly bound projectile ^{9}Be. Phys. Rev. C **99**, 034618 (2019)
24. M.E. Cage, A.J. Cole, G.J. Pyle, Ambiguities and systematics in the real central part of the optical-model potential. Nucl. Phys. A **201**, 418 (1973)
25. N. Keeley, N. Alamanos, K.W. Kemper, K. Rusek, Strong nuclear couplings as a source of Coulomb rainbow suppression. Phys. Rev. C **82**, 034606 (2010)
26. N. Otuka, E. Dupont, V. Semkova, B. Pritychenko, A.I. Blokhin, M. Aikawa, S. Babykina, M. Bossant, G. Chen, S. Dunaeva, R.A. Forrest, T. Fukahori, N. Furutachi, S. Ganesan, Z. Ge, O.O. Gritzay, M. Herman, S. Hlavac, K. Kato, B. Lalremruata, Y.O. Lee, A. Makinaga, K. Matsumoto, M. Mikhaylyukova, G. Pikulina, V.G. Pronyaev, A. Saxena, O. Schwerer, S.P. Simakov, N. Soppera, R. Suzuki, S. Takacs, X. Tao, S. Taova, F. Tarkanyi, V.V. Varlamov, J. Wang, S.C. Yang, V. Zerkin, Y. Zhuang, Towards a more complete and accurate experimental nuclear reaction data library (EXFOR): international collaboration between nuclear reaction data centres (NRDC). Nucl. Data Sheets **120**, 272 (2014)
27. A. Barioni, J.C. Zamora, V. Guimaraes, B. Paes, J. Lubian, E.F. Aguilera, J.J. Kolata, A.L. Roberts, F.D. Becchetti, A. Villano, M. Ojaruega, H. Jiang, Elastic scattering and total reaction cross sections for the ^{8}B, ^{7}Be, and ^{6}Li+^{12}C systems. Phys. Rev. C **84**, 014603 (2011)
28. V. Morcelle, R. Lichtenthaler, A. Lepine-Szily, V. Guimaraes, K.C.C. Pires, J. Lubian, D.R. Mendes Jr., P.N. de Faria, J.J. Kolata, F.D. Becchetti, H. Jiang, E.F. Aguilera, D. Lizcano, E. Martinez-Quiroz, H. Garcia, ^{8}B+^{27}Al scattering at low energies. Phys. Rev. C **95**, 014615 (2017)
29. E.F. Aguilera, E. Martinez-Quiroz, D. Lizcano, A. Gomez-Camacho, J.J. Kolata, L.O. Lamm, V. Guimaraes, R. Lichtenthaler, O. Camargo, F.D. Becchetti, H. Jiang, P.A. DeYoung, P.J. Mears, T.L. Belyaeva, Reaction cross sections for ^{8}B, ^{7}Be, and ^{6}Li+^{58}Ni near the Coulomb barrier: Proton-halo effects. Phys. Rev. C **79**, 021601(R) (2009)
30. M. Mazzocco, N. Keeley, A. Boiano, C. Boiano, M. La Commara, C. Manea, C. Parascandolo, D. Pierroutsakou, C. Signorini, E. Strano, D. Torresi, H. Yamaguchi, D. Kahl, L. Acosta, P. Di Meo,

J. P. Fernandez-Garcia, T. Glodariu, J. Grebosz, A. Guglielmetti, Y. Hirayama, N. Imai, H. Ishiyama, N. Iwasa, S. C. Jeong, H. M. Jia, Y. H. Kim, S. Kimura, S. Kubono, G. La Rana, C. J. Lin, P. Lotti, G. Marquinez-Duran, I. Martel, H. Miyatake, M. Mukai, T. Nakao, M. Nicoletto, A. Pakou, K. Rusek, Y. Sakaguchi, A. M. Sanchez-Benitez, T. Sava, O. Sgouros, V. Soukeras, F. Soramel, E. Stiliaris, L. Stroe, T. Teranishi, N. Toniolo, Y. Wakabayashi, Y. X. Watanabe, L. Yang, Y. Y. Yang, H. Q. Zhang Elastic scattering for the ^{8}B and ^{7}Be+^{208}Pb systems at near-Coulomb barrier energies. Phys. Rev. C **100**, 024602 (2019)

31. Y.Y. Yang, X. Liu, D.Y. Pang, D. Patel, R.F. Chen, J.S. Wang, P. Ma, J.B. Ma, S.L. Jin, Z. Bai, V. Guimaraes, Q. Wang, W.H. Ma, F.F. Duan, Z.H. Gao, Y.C. Yu, Z.Y. Sun, Z.G. Hu, S.W. Xu, S.T. Wang, D. Yan, Y. Zhou, Y.H. Zhang, X.H. Zhou, H.S. Xu, G.Q. Xiao, W.L. Zhan, Elastic scattering of the proton drip line nuclei ^{7}Be, ^{8}B, and ^{9}C on a lead target at energies around three times the Coulomb barriers. Phys. Rev. C **98**, 044608 (2018)
32. F.D. Becchetti, W.Z. Liu, K. Ashktorab, J.F. Bajema, J.A. Brown, J.W. Janecke, D.A. Roberts, J.J. Kolata, K.L. Lamkin, A. Morsad, R.J. Smith, X.J. Kong, R.E. Warner, Systematics of ^{8}Li-induced radioactive beam reactions: E = 13–20 MeV. Phys. Rev. C **48**, 308 (1993)
33. A. Barioni, V. Guimaraes, A. Lepine-Szily, R. Lichtenthaler, D.R. Mendes Jr., E. Crema, K.C.C. Pires, M.C. Morais, V. Morcelle, P.N. de Faria, R.P. Condori, A.M. Moro, D.S. Monteiro, J.M.B. Shorto, J. Lubian, M. Assuncao, Elastic scattering and total reaction cross sections for the ^{8}Li+^{12}C system. Phys. Rev. C **80**, 034617 (2009)
34. O.C.B. Santos, R. Lichtenthaler, K.C.C. Pires, A.M. Moro, U. Umbelino, E.O.N. Zevallos, M. Assuncao, S. Appannababu, J. Alcantara-Nunez, A.L. de Lara, V. Scarduelli, V. Guimaraes, A. Lepine-Szily, A.S. Serra, R. Linares, V.A.B. Zagatto, P.N. de Faria, V. Morcelle, M.C. Morais, A. Barioni, J.M.B. Shorto, Spin-orbit effects in the ^{8}Li+^{58}Ni elastic scattering. J. Phys. Conf. Ser. **1291**, 012030 (2019)
35. A. Pakou, D. Pierroutsakou, M. Mazzocco, L. Acosta, X. Aslanoglou, A. Boiano, C. Boiano, D. Carbone, M. Cavallaro, J. Grebosz, N. Keeley, M. La Commara, C. Manea, G. Marquinez-Duran, I. Martel, C. Parascandolo, K. Rusek, A.M. Sanchez-Benitez, O. Sgouros, C. Signorini, F. Soramel, V. Soukeras, E. Stiliaris, E. Strano, D. Torresi, A. Trzcinska, Y.X. Watanabe, H. Yamaguchi, Total reaction cross sections for ^{8}Li+^{90}Zr at near-barrier energies. Eur. Phys. J. A **51**, 55 (2015)
36. J.J. Kolata, V.Z. Golberg et al., Elastic scattering and transfer in the ^{8}Li+^{208}Pb system near the Coulomb barrier. Phys. Rev. C **65**, 054616 (2002)
37. K. J. Cook, I. P. Carter, E. C. Simpson, M. Dasgupta, D. J. Hinde, L. T. Bezzina, Sunil Kalkal, C. Sengupta, C. Simenel, B. M. A. Swinton-Bland, K. Vo-Phuoc, E. Williams. Interplay of charge clustering and weak binding in reactions of ^{8}Li. Phys. Rev. C **97** 021601(R) (2018)
38. G.R. Satchler, *Direct nuclear reactions* (Oxford University Press, Oxford, 1983)
39. M. Bhuyan, B. V. Carlson, S. K. Patra, and Shan-Gui Zhou. Surface properties of neutron-rich exotic nuclei within relativistic mean field formalisms. Phys. Rev. C **97**, 023322 (2018)
40. T. Niksic, D. Vretenar, P. Finelli, P. Ring, Relativistic Hartree–Bogoliubov model with density-dependent meson-nucleon couplings. Phys. Rev. C **66**, 024306 (2002)
41. R. Capote, M. Herman, P. Oblozinsky, P.G. Young, S. Goriely, T. Belgya, A.V. Ignatyuk, A.J. Koning, S. Hilaire, V.A. Plujko, M. Avrigeanu, O. Bersillon, M.B. Chadwick, T. Fukahori, Z. Ge, Y. Han, S. Kailas, J. Kopecky, V.M. Maslov, G. Reffo, M. Sin, ESh. Soukhovitskii, P. Talou, Reference input parameter library for calculation of nuclear reactions and nuclear data evaluation (RIPL-3). Nuclear Data Sheets **110**, 3107 (2009)
42. H. De Vries, C.W. De Jager, C. De Vries, Nuclear charge density distribution parameters from elastic electron scattering. Atomic Data Nuclear Data Tables **36**, 495 (1987)
43. G. Bertsch, J. Borysowicz, H. McManus, W.G. Love, Interactions for inelastic scattering derived from realistic potentials. Nucl. Phys. A **284**, 399 (1977)
44. A. Pakou, L. Acosta, P.D. O'Malley, S. Aguilar, E.F. Aguilera, M. Baines, D. Bardayan, F.D. Becchetti, Ch. Boomershine, M. Brodeur, F. Cappuzzello, S. Carmichael, L. Caves, E. Chavez, C. Flores-Vazquez, A. Gula, J.J. Kolata, B. Liu, D.J. Marin-Lambarri, F.F. Morales, K. Rusek, A.M. Sanchez-Benitez, O. Sgouros, V.R. Sharma, V. Soukeras, G. Souliotis, Dominance of direct reaction channels at deep sub-barrier energies for weakly bound nuclei on heavy targets: the case ^{8}B+^{208}Pb. Phys. Rev. C **102**, 031601(R) (2020)
45. M.S. Hussein, The unitarity defect of the S-matrix and the underlying absorptive potential II. The case of energy-dependent optical potentials. Ann. Phys. **177**, 58 (1987)
46. M.S. Hussein, V.L.M. Franzin, R. Franzin, A.J. Baltz, Small effects in sub-Barrier heavy-ion elastic scattering. Phys. Rev. C **30**, 184 (1984)
47. M.S. Hussein, G.R. Satchler, Halos and rainbows. Nuclear Phys. A **567**, 165 (1994)
48. B.V. Carlson, M.S. Hussein, A.K. Kerman, C.Y. Lin, Optical-model analysis of parity-nonconserving neutron-scattering at epithermal energies. Phys. Rev. C **52**, 11 (1995)
49. M.A.C. Ribeiro, L.C. Chamon, M.S. Hussein, D. Galetti, Pauli non locality in heavy-ion rainbow scattering: a further test of the folding model. Phys. Rev. Lett. **78**, 3270 (1997)
50. M.A.G. Alvares, L.C. Chamon, M.S. Hussein, D. Pereira, L.R. Gasques, E.S. Rossi, C.P. Silva, A parameter-free optical potential for heavy-ion elastics cattering process. Nucl. Phys. A **723**, 93–103 (2003)
51. L.C. Chamon, P.R.S. Gomes, M.S. Hussein, Breakup threshold anomaly: new manifestation of the dispersion relation. Phys. Rev. C **73**, 077610 (2006)